Phase Diagram of Fully Developed Drainage in Porous Media

Y. C. Yortsos* and B. Xu

Petroleum Engineering Program, Department of Chemical Engineering, University of Southern California, Los Angeles, California 90089-1211

D. Salin

Laboratoire Fluides, Automatique et Systèmes Thermiques, Université Paris VI and XI, associated with C.N.R.S. (URA 871), Batiment 502, Campus Universitaire, 91405 Orsay Cedex, France

(Received 19 June 1997)

Using concepts of invasion percolation in a gradient, we develop a phase diagram of fully developed drainage in porous media. The transition between stabilized displacement (where the conventional continuum applies) and fingering is controlled by the change of the sign of the gradient of the percolation probability (from stabilizing to destabilizing). The transition boundary is described by scaling laws. [S0031-9007(97)04702-9]

PACS numbers: 47.55.Mh, 05.40.+j, 47.55.Kf

The displacement (drainage) of a wetting (w) fluid in a porous medium by a nonwetting (nw) fluid has been analyzed in detail in the past. For drainage in an $L \times L$ pore network at constant velocity q, Lenormand [1] identified three limiting patterns, invasion percolation (IP) [2], pistonlike or compact and viscous fingering (VF) [3], and delineated their validity. As the displacement proceeds, however, spatial profiles will develop, and the overall displacement will be characterized by one of two possible global regimes, where there is a continuous transition between these limiting patterns (Fig. 1).

The first regime involves a frontal region with the structure of an IP cluster of extent σ, followed by an upstream region of increasing length with the characteristics of a compact pattern [Fig. 1(a)]. This stabilized displacement (SD) regime is where the conventional continuum description applies [4] and has been the object of many studies [5,6]. The second regime [Fig. 1(b)] has not been fully analyzed. Typically, it is described as a VF-type pattern (for example, of the diffusion-limited aggregation type) similar to miscible displacements [7]. This, however, overlooks capillarity, which at sufficiently small scales should be comparable to viscous and should affect the properties of the fingers (as, for example, in linear stability studies [8,9]). For the sake of generality, we will refer to this regime as capillary-viscous fingering (CVF).

At present, the delineation of the validity of these regimes (as well as their clear characterization) is not available. In this Letter, we provide an answer by postulating a description in terms of invasion percolation in a gradient (IPG) [10]. We particularly recognize the existence of two different global patterns, depending on whether invasion is in a *stabilizing* gradient (IPSG) or a *destabilizing* gradient (IPDG), respectively. The latter distinction is fundamental to this Letter and it is for the first time made in this context (e.g., compare to [5]).

Recall that IPG is IP in a field where the percolation probability p has a spatial gradient, typically due to a hydrostatic or permeability field, $dp/dx \sim -B$, expressed through the Bond number B. If $B > 0$, then p decreases in the direction of displacement, and the latter involves an IP frontal region of finite extent σ scaling as $\sigma \sim B^{-\frac{\nu}{\nu+1}}$, where ν is the correlation length exponent of percolation, followed by a compact region [5,10]. This is an IPSG process. In the opposite case ($B < 0$, p increasing in the direction of displacement), the process is destabilizing (IPDG) and proceeds in the form of capillary fingers, the average thickness of which also satisfies this scaling, but with $|B|$ in place of B [11]. Evidently, an IPG description would also be relevant to immiscible displacement, with the gradient now due to viscous forces. We propose that various properties of SD and CVF, the delineation of their validity, the stability of SD, and the validity of the continuum approach can be inferred by the two versions of IPG, namely, by determining the spatial variation of p and the sign of its gradient.

Consider drainage at constant volume flow rate Q in a random porous medium represented as a network of pores (e.g., $L \times N$ in 2D or $L \times L \times N$ in 3D, where N is variable). Assume constant lattice spacing l, and a pore throat size distribution $\alpha(r)$, with mean r_m and standard deviation Σr_m. In the absence of viscous forces, the displacement pattern is IP, where the front advances by penetrating the largest size throat available, and the capillary pressure $P_c = P_{\mathrm{nw}} - P_{\mathrm{w}}$ is spatially uniform [2]. In the presence of viscous forces, a gradient (negative or positive) will develop in P_c. In view of the relations $P_c = 2\gamma/r$ and $p = \int_r^\infty \alpha(r)\, dr$, where γ is the interfacial tension, this, in turn, will impart a gradient in p. Then, the process becomes one of the two versions of IPG described above. The application of IPG to infer properties of SD and CVF is detailed in [12]. Here, we briefly summarize the salient features and focus on the conditions that delineate their validity.

Consider an SD [Fig. 1(a)] and focus on the frontal region, where the pattern is IP, of width σ and lateral

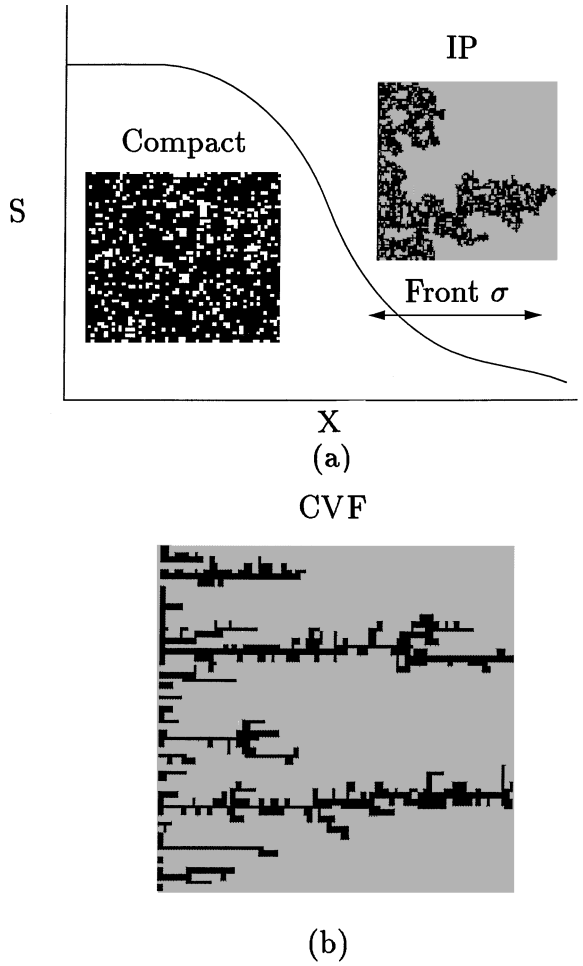

FIG. 1. Schematics of fully developed drainage: (a) Stabilized displacement (S denotes the volumetric fraction of the invading phase); (b) capillary-viscous fingering.

extent L^{d-1}, where d is the embedding dimension. This region is centered around the mean front position $X_c(t)$, traveling at velocity v, and defined, in analogy with IPG, as the place where the transverse average of p is equal to the percolation threshold, $p(X_c) = p_c$. It is shown in [12] that use of IPSG results in the following equation for σ:

$$\left(b\sigma^{\frac{\zeta+\nu(D-1)}{\nu}} - M\sigma\right) \sim \frac{2\Sigma}{\mathrm{Ca}_F}\,\sigma^{-\frac{1}{\nu}}, \qquad (1)$$

where $M = \mu_w/\mu_{nw}$ is the viscosity ratio, $\mathrm{Ca}_F = v\mu_{nw}/\gamma$ is the capillary number at the front, and b is a dimensionless constant. Exponents ζ and D correspond to the conductance and the mass fractal dimension of the percolation cluster, respectively [13]. Upstream of the front, there is a compact region [Fig. 1(a)], the transition to which can be described by a crossover function [12].

Equation (1) is obtained by applying the self-consistency argument of gradient percolation [5,10], which states that since σ delineates the extent of the IP cluster, we must also have $\Delta p \sim \sigma^{-\frac{1}{\nu}}$, where Δp ($\equiv -\sigma\frac{dp}{dx}$) is the variation of p in that region, namely, $\Delta p \sim \mathrm{Ca}_F/2\Sigma(b\sigma^{\frac{\zeta+\nu(D-1)}{\nu}} - M\sigma)$. The latter, in turn, is obtained by using the relation between P_c and p, referred to above, and the expression for the change in capillary pressure, $\Delta P_c \sim v\mu_{nw}/r_m\sigma(b\sigma^{\frac{\zeta+\nu(D-2)}{\nu}} - M)$, obtained by estimating the pressure drops in this region [12]. Essentially, the term between the brackets of ΔP_c, and Δp, and of (1) expresses the difference between the pressure drops in the nw and w phases. The power law reflects the progressively increasing resistance to flow of the nw phase, which occupies part of a percolation cluster, as its size increases.

It is easily shown that (1) admits a unique positive solution for *all* values of M and Ca_F. At small Ca_F, this solution approaches the power-law asymptote $\sigma \sim (\mathrm{Ca}_F/2\Sigma)^{-\frac{\nu}{1+\zeta+\nu(D-1)}}$, which has an exponent identical to Wilkinson's [5]. However, his result was obtained differently, by extrapolating in the frontal *fractal* region a *continuum* solution, valid behind the front. It is interesting to note from (1) that an increase in the disorder of the pore structure (increasing Σ) has an effect which is equivalent to an increase in capillarity.

The fact that a solution of (1) exists for all M and Ca_F also means that fully developed SD exists (but is not necessarily stable) for all M and Ca_F (because of the existence of a solution, the left-hand side (LHS) of (1) is positive, hence p decreases in the direction of displacement). To establish whether this regime will actually develop, however, we must address its stability. Equivalently, this can be done by examining the development of the *initial* phase of the displacement, before a traveling-wave solution develops. An analysis of the properties of the CVF regime is given in Ref. [12].

Consider, now, the delineation of the validity of these regimes, in which case one needs to address the *initial* phase of the displacement. During this interval, the displacement has an extent $\chi(t) \times L^{d-1}$, where χ is increasing with time. The pattern is of the IP type as long as $\chi(t) \leq \chi_\epsilon(\mathrm{Ca}, M)$, where $\chi_\epsilon(\mathrm{Ca}, M)$ is to be determined. At $\chi = \chi_\epsilon$, the pattern departs from percolation and a transition towards a fully developed displacement starts. The latter will either become a SD (with a compact region following an IP front) or a CVF regime, depending on whether, at χ_ϵ, p decreases or increases in the direction of displacement, respectively. To trace this transition, we need, first, to identify χ_ϵ and, second, to determine the sign of the gradient of p at that point.

The analysis is similar to the SD case. The pressure drops are expressed similarly, but now with χ in place of σ and $Q_{nw} = Q$ (there are no traveling fronts). Note also that a slight modification is needed because here the entire cluster is fractal. As previously, the most important quantities are ΔP_c and Δp across a region of

extent χ, which in absolute value is read as $|\Delta P_c| \sim 2\gamma\Sigma/r_m|\Delta p| \sim q\mu_{\rm nw}/r_m|c\chi^{\frac{\zeta+\nu(d-1)}{\nu}} - M\chi|$, where c is another constant. To define χ_ϵ, we follow Lenormand [1] and request that at χ_ϵ, we must have $|\frac{\Delta N_p}{N_p}| = \epsilon \ll 1$, where N_p is the fraction of sites of the nw phase occupying an IP cluster. The scaling of the latter can be obtained from percolation theory, namely, $N_p \sim (\text{const})\,(p - p_c)^\beta$ [13]. Proceeding as in [1], substituting $|\Delta p| = |p - p_c|$ from the above, and taking $\chi = \chi_\epsilon$, gives the following equation:

$$\frac{\rm Ca}{\Sigma}\chi_\epsilon^{\frac{1+\nu}{\nu}}|c\chi_\epsilon^{\frac{\zeta+\nu(D-2)}{\nu}} - M| \sim \epsilon\,, \qquad (2)$$

the solution of which will be discussed below. This equation represents a generalization of the two equations of [1] describing the IP-to-compact and IP-to-VF boundaries, respectively (which were determined in [1] in what amounts to a $\chi_\epsilon \times \chi_\epsilon$ lattice under the assumption that pressure drops occur only in one phase).

We note that in (2), $c\chi_\epsilon^{\frac{\zeta+\nu(D-2)}{\nu}}$ actually represents the large-χ asymptote of the ratio $M\Delta P_{\rm nw}/\Delta P_{\rm w}$. When the lattice is finite or when χ_ϵ is small, a more general expression, to be obtained numerically, must be used. Using 3D pore network simulations, we computed this ratio, as shown in the inset of Fig. 2 (actually, we computed its equivalent ratio of the two flow conductances $G_{\rm w}/G_{\rm nw}$ at $M = 1$). At relatively large χ, the curve has the expected power-law scaling, although it eventually reaches a plateau, which reflects finite-size effects. For sufficiently small χ, the curve approaches a realization-dependent value M^*. For the purposes of this Letter, we will assume in the remaining that L and χ_ϵ are sufficiently large for the power-law scaling of percolation in (2) to be applicable (as shown in Fig. 2). We will also take $M^* = 1$, for reasons to be discussed below.

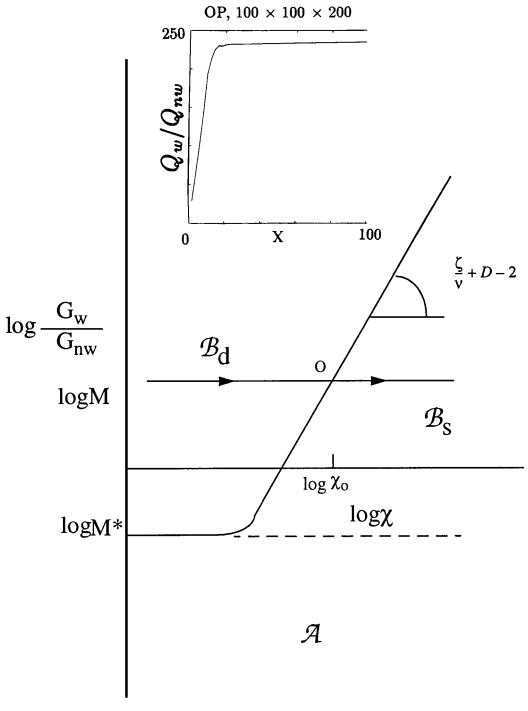

FIG. 2. The ratio $M\Delta P_{\rm nw}/\Delta P_{\rm w}$ [first term between brackets in (2)] vs the extent χ_ϵ. In the inset are results from simulations in a $100 \times 100 \times 200$ pore network.

The solution of (2) depends on the sign of $c\chi_\epsilon^{\frac{\zeta+\nu(D-2)}{\nu}} - M$. It is apparent from Fig. 2 that we must distinguish two different cases:

(a) If $M < M^*$ (region $\mathcal{A}$ in Fig. 2), the term between the brackets in (2) is positive, and the resulting equation is very similar to (1) describing the extent of the stabilized zone in SD. As in that case, it admits a solution for *all* values of Ca, with the same dependence on parameters as σ. Moreover, and for the same reasons as in SD, p is decreasing with distance for all $\chi(t) \le \chi_\epsilon$, and the problem is IPSG. This means that when χ_ϵ is reached, the regime that will set in will be an SD. Thus, when $M < M^*$, the displacement is an *unconditionally* stabilized displacement. This conclusion is similar to that of conventional stability analyses [8] (where $M^* = 1$), but it is reached here using IPG.

(b) If $M > M^*$, the solution χ_ϵ can lie either in region $\mathcal{B}_d$ or in region $\mathcal{B}_s$ (Fig. 2). If in $\mathcal{B}_d$, the term in the brackets of (2) is negative, which means that p *increases* with distance (note that Δp has the same sign as $c\chi_\epsilon^{\frac{\zeta+\nu(D-2)}{\nu}} - M$). In this case, therefore, the pattern at χ_ϵ will tend toward the CVF regime. Now, χ_ϵ solves the different equation

$$-\chi_\epsilon^{\frac{1+\nu}{\nu}}\left(c\chi_\epsilon^{\frac{\zeta+\nu(D-2)}{\nu}} - M\right) \sim \frac{\Sigma}{\rm Ca}\,\epsilon\,. \qquad (3)$$

However, and contrary to case (a), a solution of (3) *does not* exist for all M or Ca. Indeed, its LHS goes through a maximum as a function of χ, which, when substituted back in (3) gives the following condition for a solution to exist:

$$\frac{\rm Ca}{\Sigma}M^{\frac{\zeta+1+\nu(D-1)}{\zeta+\nu(D-2)}} \ge O(\epsilon) \qquad (4)$$

[where we grouped all constants into an $O(1)$ parameter]. Equivalently, (4) expresses the condition for the existence of the CVF regime. It shows that for M above M^*, the displacement will become CVF provided that Ca or M are sufficiently large. Otherwise, the pattern will remain at percolation as the displacement proceeds throughout region $\mathcal{B}_d$ [since a solution to (3) will *not* exist], as well as *after* $\mathcal{B}_d$ is exited (at χ_0, Fig. 2) and region $\mathcal{B}_s$ is entered. In the latter region, the term within the brackets in (2) is positive, the resulting equation having a solution for *all* values of M or Ca. Reasoning as in case (a), we conclude that if (4) is violated, the transition will be toward a SD.

We summarize the above as follows: A stabilized displacement is possible either if $M < M^*$ for all Ca, or if

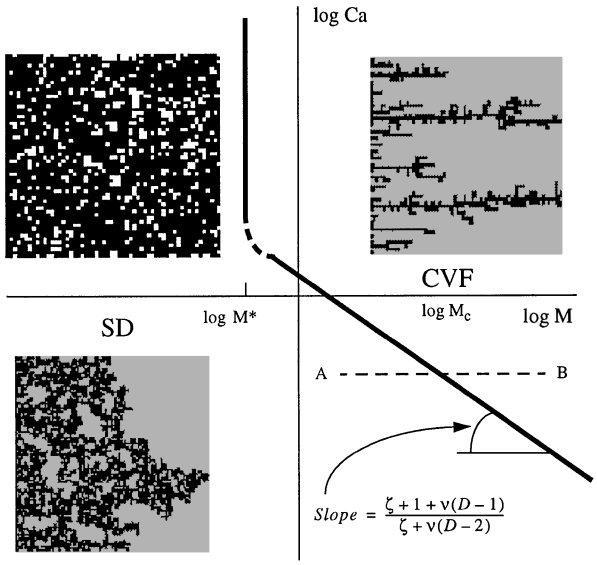

FIG. 3. Phase diagram of fully developed displacement in drainage.

$M > M^*$ but for sufficiently small Ca, as dictated by (4). Otherwise, the displacement will be destabilized. These results can be portrayed in a phase diagram of fully developed drainage with axis ln Ca and ln M (Fig. 3). The two regimes SD and CVF are separated by a line, which at large M is asymptotically straight with slope $\frac{\zeta+1+\nu(D-1)}{\zeta+\nu(D-2)}$, and as M approaches M^* becomes asymptotically vertical. Because at large Ca, the boundary delineating SD from CVF must be the vertical line $M = 1$, by extension we take $M^* = 1$ (see also [14]). We note that the curve separating the two regions also serves to delineate the validity of the conventional continuum description, which only applies to a SD displacement. This provides a resolution of a long-standing question.

It is interesting to consider the variation of χ_ϵ as we cross the transition from SD to CVF (for example, by increasing M along the path AB of Fig. 3). A schematic of the solution of (2) in the two cases when the quantity in brackets is positive (case of SD) or negative (case of CVF), respectively, is shown in Fig. 4. [A simple qualitative analog would be to replace (2) by the quadratic $|c\chi_\epsilon^2 - M\chi_\epsilon| = a$.] On the SD (stable) side, the solution increases monotonically with M. On the CVF side, however, there exist two branches, one increasing and the other decreasing with an increase in M. It is the lower branch which will be selected, as in a transient displacement it is the smaller χ_ϵ which will be encountered first. Thus, when the critical curve is reached (at M_c), there is a discontinuity, which here indicates a first-order phase transition. This interesting behavior is also the result of the application of IPG to the problem.

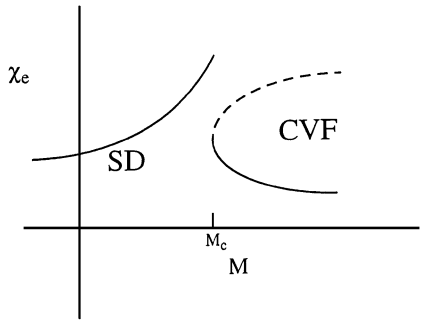

FIG. 4. Schematic of the variation of χ_ϵ (at which there is departure from IP towards either SD or CVF) as a function of M for constant Ca (following path AB in Fig. 3). Note the first-orderlike phase transition at the critical point. The dashed-line branch on the CVF side is not reached.

The research of Y. C. Y. was partly supported by DOE Contract No. DE-FG22-96BC1994/SUB and by an Invited Professor appointment at UPMC and UPS.

*To whom correspondence should be addressed.

[1] R. Lenormand, Proc. R. Soc. London A **423**, 159 (1989).
[2] R. Lenormand and S. Bories, C. R. Hebd. Seances Acad. Sci. B (Paris) **291**, 279 (1980); R. Chandler, J. Koplik, K. Lerman, and J. F. Willemsen, J. Fluid Mech. **119**, 244 (1982); D. Wilkinson and J. F. Willemsen, J. Phys. A **16**, 3365 (1983).
[3] T. A. Witten and L. M. Sander, Phys. Rev. B **27**, 5686 (1983); G. M. Homsy, Annu. Rev. Fluid Mech. **19**, 271 (1987).
[4] L. W. Lake, *Enhanced Oil Recovery* (Prentice-Hall, Englewood Cliffs, NJ, 1989).
[5] D. Wilkinson, Phys. Rev. A **30**, 520 (1984); D. Wilkinson, Phys. Rev. A **34**, 1380 (1986).
[6] M. Blunt, M. J. King, and H. Sher, Phys. Rev. A **46**, 7680 (1992).
[7] M. J. King and H. Sher, Phys. Rev. A **41**, 874 (1990); M. Ferer, W. N. Sams, R. A. Geisbrecht, and D. H. Smith, AIChE. J. **41**, 749 (1995).
[8] R. L. Chuoke, P. van Meurs, and L. B. van der Poel, Trans. AIME **216**, 188 (1959); Y. C. Yortsos and F. J. Hickernell, SIAM J. Appl. Math. **49**, 730 (1989).
[9] R. Combescot, T. Dombre, V. Hakim, Y. Pomeau, and A. Pumir, Phys. Rev. Lett. **56**, 2036 (1986); S. Tanveer, Phys. Fluids **30**, 2318 (1987).
[10] J. F. Gouyet, B. Sapoval, and M. Rosso, Phys. Rev. B **37**, 1832 (1988); J.-P. Hulin, E. Clement, C. Baudet, J. F. Gouyet, and M. Rosso, Phys. Rev. Lett. **61**, 333 (1988); M. Chaouche, N. Rakotomalala, D. Salin, B. Xu, and Y. C. Yortsos, Phys. Rev. E **49**, 4133 (1994).
[11] V. Frette, J. Feder, T. Jossang, and P. Meakin, Phys. Rev. Lett. **68**, 3164 (1992); P. Meakin, J. Feder, V. Frette, and T. Jossang, Phys. Rev. A **46**, 3357 (1992).
[12] B. Xu, Y. C. Yortsos, and D. Salin, Phys. Rev. E (to be published).
[13] D. Stauffer and A. Aharony, *Introduction to Percolation Theory* (Francis-Taylor, London, 1992).
[14] In actuality, condition (4) needs to be modified near M^*, where χ_ϵ is small and the percolation scalings do not strictly apply. Near M^*, condition (4) would involve $M - M^*$ and a dependence different than shown.